AC AND DC CURRENT DEPENDENCE OF ON-CHIP INDUCTORS

Emily Wesseling, Erik Brandon , and Udo Lieneweg
Center for Integrated Space Microsystems
Jet Propulsion Laboratory
California Institute of Technology
4800 Oak Grove Dr., Pasadena, CA 91109

Rahman Rub, Sukirti Gupta, Tae Chul Nam,
and Chong H. Ahn
University of Cincinnati
Dept. of Electrical and Computer Engineering and Computer Science
PO Box 210030, Cincinnati, OH 45221

ABSTRACT

The prospect of a monolithic, integrated dc-dc converter has spurred the development in on-chip inductors using conventional silicon compatible fabrication techniques. In these converters, the inductor's ability to perform while sustaining a dc current is vital. Because the permeability of magnetic materials is in general a highly nonlinear function of the applied field, the properties of inductors with magnetic cores depend on the amplitude of the oscillating current and any dc current through them. We have characterized toroidal MEMS inductors and encapsulated spiral inductors as a function of those applied currents.

INTRODUCTION

Further miniaturization of very robust, small spacecraft is hampered by the large size of radiation-tolerant dc-dc converters. Most spacecraft need several of these because the voltage generated on-board is 24-28 Vdc while many electronics and MEMS systems need either lower or higher voltages. Moreover, duplicate converters may be desired to increase overall reliability. Radiation-tolerant dc-dc converters are bulky and far from monolithic because they rely on large, discrete passive components, especially inductors and transformers. Much effort has gone into developing miniaturized magnetic components suitable for future dc-dc converters using conventional silicon compatible fabrication techniques (1 – 7). We are continuing that work to learn how to tailor such microinductors (and microtransformers) for particular dc-dc converters. Typical inductors for converters operating at 1 to 10 MHz will need inductances of 1 to 10 μH and resistances below 1 Ω. To realistically compete with surface mount devices, a microinductor should occupy a footprint on the order of a few square millimeters, or less, and be fabricated by low temperature methods. Moreover, energy storage inductors must provide adequate filtering while carrying a DC current as the inductor must source all the current through the load in a dc-dc converter. For future low-power applications, this direct current may be on the order of 100 mA with a ripple current through the inductor

about 10 mA peak-to-peak. Current can degrade microinductor performance through heating, electromigration, and saturation of the magnetic core. Heat dissipation from these devices may be a problem due to their small surface area. Electromigration effects in the thick copper metallization through the new dielectrics which microinductors require, is an important issue for their long-term reliability. A key limiting factor at present, however, is the current's influence on the inductors' performance through the magnetization-field characteristics of the magnetic core. Inductors without magnetic cores avoid this problem, operate well to high frequencies, and are relatively simple to fabricate; however, it is not possible to achieve an adequate inductance per unit volume with these "air core" inductors for dc-dc converter applications.

Microinductors take two basic forms: solenoids, where the conductor is wrapped around a core, and encapsulated spirals or pot-cores where the magnetic core surrounds the conductors. An example of the first kind is the microinductor shown in Figure 1, which has a toroidal core with a gap in it. Pot-core microinductors or "encapsulated spirals" are simple spiral traces sandwiched by dielectric and magnetic layers, as shown schematically in Figure 2.

As review, we relate a device's inductance to the hysteresis loop of its core. (We should use a hysteresis loop measured with the ramp rate of the applied field equal to the rate of change of current through the inductor.) In the hysteresis loop, the y-axis is the magnetic flux density, $B = \mu_0 (H + M)$, where μ_0 is the permeability of free space, H is the applied field and M is the magnetization or magnetic moment per unit volume, and the x-axis is the applied field, H. The slope of a curve on this graph is the relative permeability of the material,
$\mu_r = \Delta B / \Delta H$. If we consider this material as the core of an inductor, the inductance, L, is measured in the time domain as

$$L = \int V_i \, dt / I, \qquad [1]$$

where V_i is the induced voltage and I the current through the inductor. The induced voltage differs from the terminal voltage by the voltage drop over the coil resistance R, i.e.,

$$V_i = V - R I. \qquad [2]$$

If the same magnetic flux Φ flows through all N turns of the coil, then

$$L = N \Phi / I. \qquad [3]$$

If, furthermore, the field and the flux density are uniform, then

$$L = N B \cdot A / I = N B \cdot A / (H / (N/l)) \qquad [4]$$

where A is the cross-section of the core and l its length. The magnetic field, H, applied to the core will be proportional to the current with a constant of proportionality determined

by the geometry of the coils. We see that if the y-values on the B-H plot are multiplied by N A and the x values are divided by the geometric factor N/l, the resulting graph of $\int V_i\,dt$ versus current has the same shape as the material's B-H loop. The slope of the new curve is the inductance. Clearly, a simple way to increase the amount of current necessary to saturate the core is through the geometric factor between H and I, i.e., use fewer turns per unit length. This approach can decrease the resistance of the coil, but it also reduces the inductance per unit volume. As usual, the area enclosed by the loop is the energy lost.

Although the onset of saturation in the core, and degradation of inductor performance, is determined by the peak current, $I_{dc}+ (1/2)\ I_{peak\text{-}to\text{-}peak}$, the dependence of the measured inductance on the bias and alternating current is subtle. Figures 3 through 5 show typical dependencies of the inductance on alternating and direct current levels. The actual x and y scales on these plots will differ for different micro- and discrete inductors, but the overall trends will be the same. Figure 3 illustrates typical behavior of an inductor with a magnetic core as a function of increasing AC field with no DC bias. With a small alternating current, the material cycles around some minor loop, which may depend on the applied field history. With increased current amplitude, most of the major loop will be traversed, and the inductance will be maximum. If the amplitude of the alternating current is increased further, the material is in saturation part of the time, so the inductance decreases. Figure 4 illustrates the effect of increasing DC bias with an AC current slightly too small to drive the core into saturation. At zero DC current, most of the hysteresis loop is traversed, and the inductance is high. As the bias increases, the material spends more and more of the cycle saturated, and the inductance decreases. Finally, Figure 5 illustrates the combined influence of AC and DC current level. With small alternating current the device behaves as just described, going from high to low inductance near the point where the DC current saturates the core. However, with a large alternating current the core is saturated for a significant portion of the cycle at zero DC bias, and that proportion, and thus the intermediate-value inductance, remains the same over a relatively wide range of DC bias. The losses follow curves similar to those of the inductance. The area of the hysteresis loop that is swept out represents a loss, which is added to the resistance of the coil, but no magnetic losses are generated when the material is saturated.

The inductor core should be designed such that the field generated by the current must rotate the magnetization away from an energy minimum. Magnetization response through rotation, not domain wall motion, is preferred because it can be lossless and remain constant from DC to higher frequencies. Note that increasing the saturation field without increasing the magnetization inevitably leads to lower permeability and lower inductance per unit volume. The magnetic energy density of a core of soft amorphous or polycrystalline material is the sum of four terms. They are the magnetostrictive, the magnetic field, the induced anisotropy, and the demagnetization energy densities. The magnetostrictive term arises from the coupling between the magnetization and the stress in the material. For good soft magnetic properties and consistently good performance in integrated devices, materials with magnetostriction (coupling) coefficients of zero are desired. However, since these are generally finite, magnetostriction has been used to increase the anisotropy in some recording heads. The magnetic field energy density is simply the energy of the magnetization in an external field, which is generated by any currents or magnets nearby. Sanders has suggested supplementing the induced uniaxial

anisotropy field with the field from permanent magnets incorporated into a microinductor or using permanent magnets alone in an inductor embedded in printed wiring board to align the magnetization (8, 9). The induced uniaxial anisotropy arises from directional ordering of magnetic ions under the influence of an external field during deposition or annealing. The demagnetization energy density comes from the interaction of the magnetization with the field from the free poles which are produced where the magnetization of a specimen intersects its surface. The energy density of any core will generally contain some combination of these effects.

The induced uniaxial anisotropy field is difficult to use effectively because the orienting field is applied across the entire wafer, creating one easy axis for all the material deposited or annealed at that time. This obviously poses a problem for toroidal cores. Pot cores can be stretched in one direction and left open at the ends so that the coil resembles a racetrack with only the straight parts covered by core material. Other designs, such as the meander coil, and the "magnetically coated wire" have been devised to increase the percent of the current path lying in one direction (10, 11).

In contrast to the induced uniaxial anisotropy, the demagnetizing field does not take a fixed direction on the wafer. It is always directed opposite the magnetization inside the specimen. It is controlled through shaping, or patterning, the core material. The best known example is the insertion of a gap in a toroidal core. This design has the disadvantage that stray or fringing fields may emanate from the gap and produce electromagnetic interference in nearby components. In an encapsulated spiral one or both dielectric layers may be extended to create a gap between the upper and lower magnetic layers. In Figure 6 the lower dielectric layer can be seen separating the upper magnetic layer from the lower. Bringing the two layers together in a precise manner and leaving a reproducible gap depends on good control of the dielectrics. This is particularly challenging when spun-on, polymer dielectrics are used because they can flow. Patterning the individual magnetic layers also provides shape demagnetization fields although this patterning is generally introduced to break up eddy currents.

EXPERIMENTAL

All measurements were taken with a Hewlett Packard 4284A impedance analyzer. The analyzer generates a sine wave excitation and was operated in Automatic Level Control mode, where the measured value of the current across the device under test is kept constant. Inductance and series resistance are extracted from the imaginary and real parts of the measured impedance

$$Z = j\,2\,\pi\,f\,L + R_s(f). \qquad [5]$$

Here the series resistance $R_s(f)$ models not only the coil resistance but also the previously mentioned hysteresis loss and eddy current losses. In order to keep the core losses down, the measurements should be performed at a relatively low frequency. A sequence of data points was recorded with generally increasing DC or AC current, with periodic remeasurement of the response at zero DC or 1 mA rms and 15 mA. The small

alternating field, no DC bias values agree well with those measured on a network analyzer (HP8753B,) as expected. In a quantitative analysis it should be kept in mind that the inductance extracted in the frequency domain (Eq. 5) may be smaller than that extracted in the time domain (Eq. 1) when the core is driven into saturation. The frequency analysis regards only the fundamental of the induced voltage and neglects harmonics.

This work addressed two sets of inductors: toroid inductors fabricated at the University of Cincinnati and encapsulated spiral inductors fabricated at the Jet Propulsion Laboratory. The process for fabricating these toroidal inductors is based on a well established process at the University of Cincinnati involving thick photolithography techniques combined with the electroplating of copper conductors and Permalloy magnetic cores. Moreover, these toroidal inductors without air-gaps are amenable to analysis using simple approximations, as discussed above.

The toroidal inductors were fabricated as described in (12). Their outer dimensions are 4 mm by 1.5 mm by 120 μm with 70-turn copper coils plated around a Permalloy core. No field was applied during the deposition of the cores. Figure 7 presents the inductance of inductors with the three types of cores; solid, laminated, and gapped; as a function of DC bias with an exciting current of 10 mA rms at 1 kHz. This amplitude was chosen for convenience and for comparison with previous studies. The gapped inductors resemble the device in Figure 1. The gaps are on the order of 40 μm long.

A set of encapsulated spiral test structures has been designed at JPL to empirically determine the dependence of the inductor performance on certain design parameters, such as inductor aspect ratio or the extent of dielectric and ferromagnetic layers, and to develop robust fabrication processes for both electroplated Permalloy and sputtered CoZr core materials. Data from one set, with a 15-μm thick copper conductor and electroplated Permalloy core layers, are presented here. No field was applied during deposition of the Permalloy. Details of the fabrication are in (13). Their inductances at 1 MHz are 4 to 10 times greater than they would be without a magnetic core. The AC current dependence of one with a ten-fold enhancement of its inductance is shown in Figure 8, and its inductance as a function of AC and DC currents in Figure 9. This coil has ten 15-μm-wide turns separated by 10 μm edge-to-edge in a 0.6 mm by 1.0 mm footprint. The Permalloy core encloses the coil completely except for four 15-μm-wide slits to break up image currents. Both dielectric layers extended 20 μm beyond the coils. The ferromagnetic layers extend 20 μm further from the coils than the dielectric layers. The inductance as a function of DC bias, at 10 mA rms, for this and several other inductors from this set are shown in Figure 10.

DISCUSSION

The low frequency inductance of the solid core toroidal inductor is easily calculated using the geometry of the device and a permeability estimated from the quasistatic M-H loop measured with a vibrating sample magnetometer. The permeability at high frequencies may be lower. Because the core is closed, the demagnetization factor is zero.

Because the permeability of the Permalloy is much greater than that of the dielectric, the flux will essentially be confined to the core. Thus:

$$L = \mu_o \mu_r A_c N^2 / l_c \approx 17 \times 10^{-6} H \quad [6]$$

where:

$\mu_o = 4\pi 10^{-7}$ H/m ; the permeability of free space

$\mu_r = 4 \times 10^3$; the relative permeability of the core

$A_c = 25 \times 10^{-6} \times 280 \times 10^{-6}$ m^2 ; the cross-sectional area of the core;

$N = 70$; the number of turns

$l_c = 10^{-2}$ m; the length of the core

In Figure 7 both closed cores, solid and laminated, start losing inductance with about 7.5 mA dc. This is consistent with the hysteresis loops. The field generated by the dc current flowing through 70 turns on a 1 cm long core is approximately 52 A/m or 0.7 Oe, and the peak field is 151 A/m or 1.9 Oe. The zero bias inductance and the saturation current level for the ungapped cores, both solid and laminated, fit the model well. The gapped core, however, cannot be described by the simple equation where the effective permeability of the core is reduced by a factor of $(1 + \mu_r l_g/l_c)$

$$L = \mu_o \mu_r A_c N^2 / (l_c (1 + \mu_r l_g/l_c)) \quad [7]$$

where l_g is the length of the gap (14). From this approximation, the 40-μm gap should decrease the inductance and increase the saturation field by a factor of 16. Instead the gapped core has a zero bias inductance about half that of the solid core and about twice the saturation current. Considering the actual structure of this inductor, it is apparent that this simple approximation is inadequate. The model assumes that all the flux goes directly from one pole-face to the other through an area equal to that of the pole-face. This requires that the gap length be much smaller than any other dimension of the core. In this microinductor, though, the thickness of the core is 25 μm, less than the gap length, and so much of the flux is expected to fringe outside the gap. Although this core thickness does not represent the ultimate limit of electrodeposited materials, even discrete inductors with gaps less a tenth of either cross-sectional dimension require more complex models to account for fringing flux. In practice, 3-dimensional finite element modeling must be employed to accurately predict the performance of toroidal microinductors. Such modeling efforts are underway at the University of Cincinnati.

The fields in pot-core or encapsulated spiral inductors are more difficult to analyze than those in toroids, although the low frequency inductance of a bare metal spiral is easily calculated. Again, better analytic expressions and 3-D models are being developed. A few conclusions may be drawn from the data shown in Figures 8 through 10. First, the inductor with the greatest, 10-fold, enhancement of its inductance over that of the coil in air also shows strong dependence on DC-bias and on the alternating current. Presumably this enhancement comes from good enclosure of the field, a low demagnetization factor. Second, those with only a six-fold or so enhancement retain at least 70% of their zero-bias inductance with 100 mA DC. Finally, the device that achieves a similar inductance (400 nH) in a much larger area, 6 mm^2 instead of 0.6 mm^2, through the use of a few wide turns, shows almost no dependence on DC bias from 0 to 100 mA.

CONCLUSIONS

As with discrete inductors, the level of direct current which must be sustained by the component is an important parameter in designing microinductors and often entails compromises in other attributes, such as reduced inductance per unit volume or increased electromagnetic interference. Many routes are available to improve microinductor performance over these preliminary results. These include precise control of the space between upper and lower ferromagnetic layers in encapsulated spiral inductors and inducing uniaxial anisotropy in the core material. These methods increase the saturation field of the material and necessarily decrease its permeability. Switching to materials with higher saturation magnetization will help. However, the maximum magnetization obtainable is about 2.4 times that of Permalloy while saturation fields approximately 10 times that of isotropic Permalloy are needed. Accurate prediction of inductor performance from design and fabrication parameters will require more data, including the variation of frequency in the current-dependent impedance measurements, and more advanced modeling. Nevertheless, microinductors applicable to low-power dc-dc converters, carrying 100 mA DC, appear feasible.

ACKNOWLEDGEMENTS

The authors wish to acknowledge the support of the NASA Deep Space Systems Technology Program and the JPL Center for Integrated Space Microsystems, as well as Dr. Trifon Liakopoulis for designing the toroidal inductors and Ken Evans for the cross-sectional SEM.

REFERENCES

1. C. H. Ahn, Y. J. Kim, M. G. Allen, *IEEE T Compon. Pack. A,* **17,** 463, (1994).
2. T. Sato, H. Tomita, A. Sawabe, T. Inoue, T. Mizoguchi and M. Sahashi, *IEEE Trans. Magn.*, **30**, 217 (1994).
3. Y Sasaki, S Morita, T Hatanai, A Makino, T Sato, K Yamasawa, *Nanostruct. Mater.*, **8,** 1025, (1997).
4. T Sato, Y Miura, S Matsumura, K Yamasawa, S Morita, Y Sasaki, T Hatanai, A Makino, *J Appl. Phys.*, **83,** 6658, (1998).
5. J. Y. Park, M. G. Allen, *IEEE T Electron. Pa M,* **23,** 48, (2000).
6. S. Sugahara, Z. Hayashi, M. Edo, Y. Katayama, M. Gikinozu, K. Matsuzaki, A. Matsuda, E. Yonzawa, K. Kuroki, *IPEC Tokyo 2000*, 326 (2000).
7. D. H. Shin, C. S. Kim, J. H. Jeong, S. Bae, S. E. Nam, and H. J. Kim, *J. Appl. Phys.*, **87,** 5854 (2000).
8. L. Daniel, C. R. Sullivan, and S. R. Sanders, *IEEE Trans. Power Electronics* **14,** 709, (1999).
9. Y. I. Zhang and S. R. Sanders, *PESC 99, 36th Annual IEEE,* 561, (1999).

10. K. Kawabe, H. Koyama, and K. Shirae, *IEEE Trans. Magn.*, **20**, 1804 (1984).
11. V. Korenivski and R.B. van Dover, *J. Appl. Phys.*, **82**, 5247 (1997).
12. T. M. Liakopoulos and C. H. Ahn, *IEEE Trans. Magn.*, **35**, 3679 (1999).
13. E. Brandon, E. Wesseling, V. White, U. Lieneweg, H. Cherry, J. Podosek, and A. Hernandez-Pellerano, these proceedings.
14. J. K. Watson, *Applications of Magnetism*, p. 135, Wiley-Interscience, New York (1980).

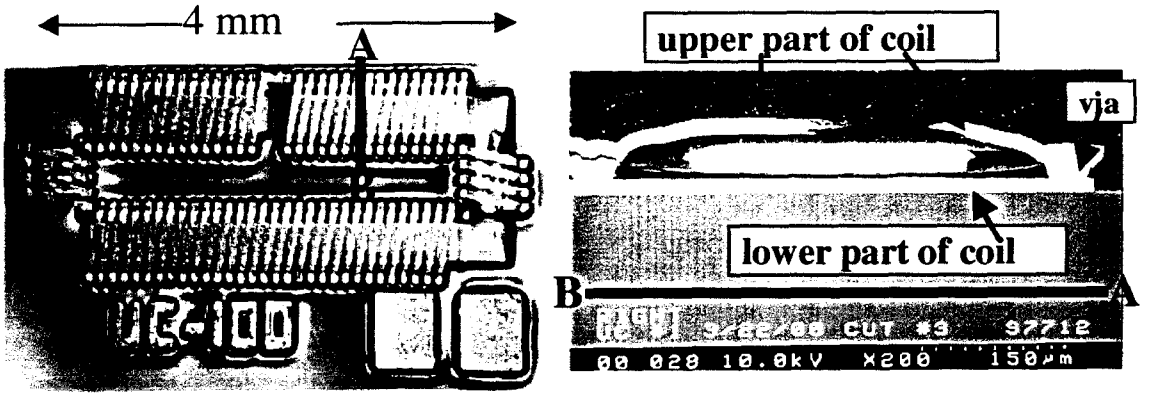

Figure 1 Left: top view photograph of toroidal microinductor. Right: Cross-sectional Scanning Electron Micrograph of the toroidal microinductr.

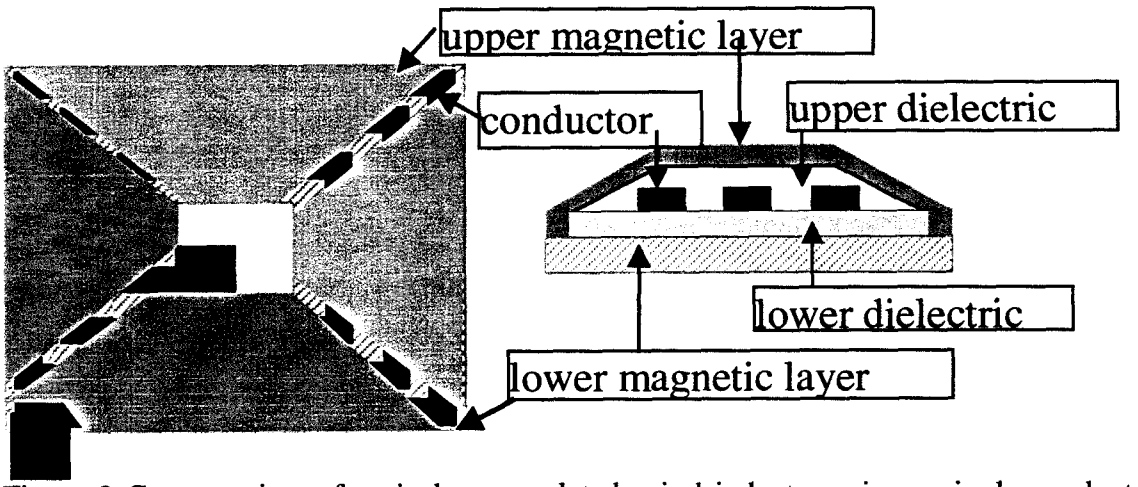

Figure 2 Cartoon view of typical encapsulated spiral inductor using a single conductor layer. Left: Top view. The dielectrics are not shown. One contact pad is on the outside and one is in the middle. The upper ferromagnetic layer is divided into four segments. Right: Cross-section showing all 5 layers, not to scale.

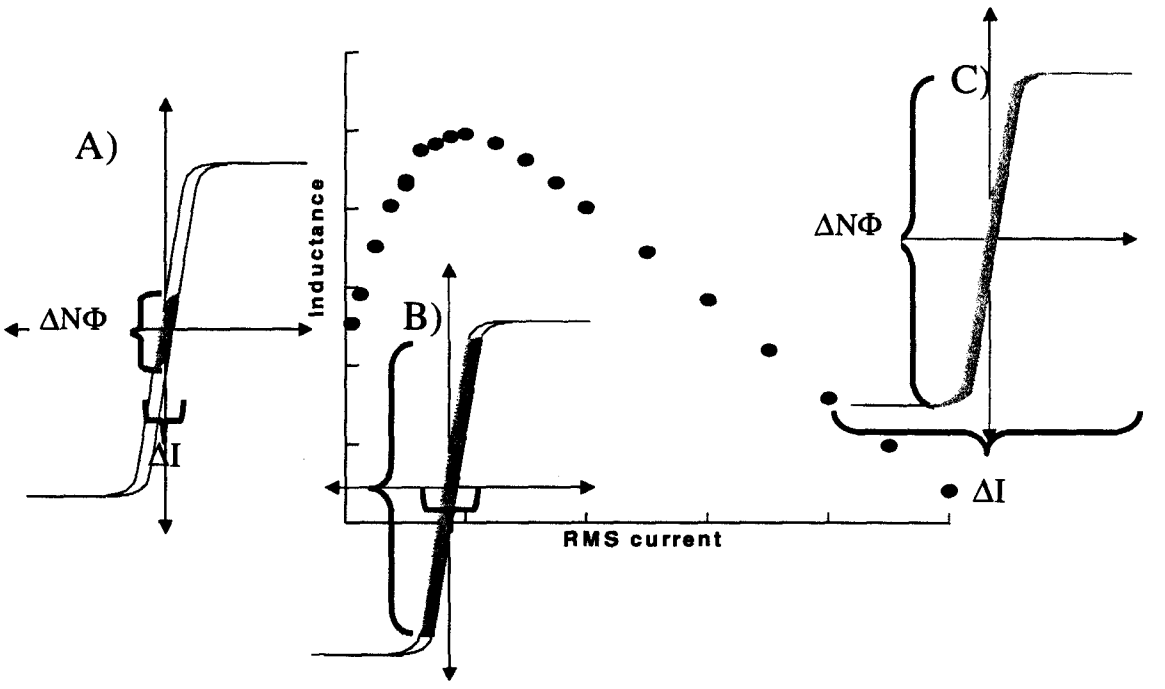

Figure 3 Inductance as a function of alternating current for a typical magnetic core inductor. A) At low AC levels, a minor hysteresis loop is traced out; so, the change in flux per unit current is small. B) The inductance is maximum when the entire major loop is traversed. C) As the material goes into saturation, the change in flux increases very little, although the amplitude of the current continues to increase, and the inductance decreases.

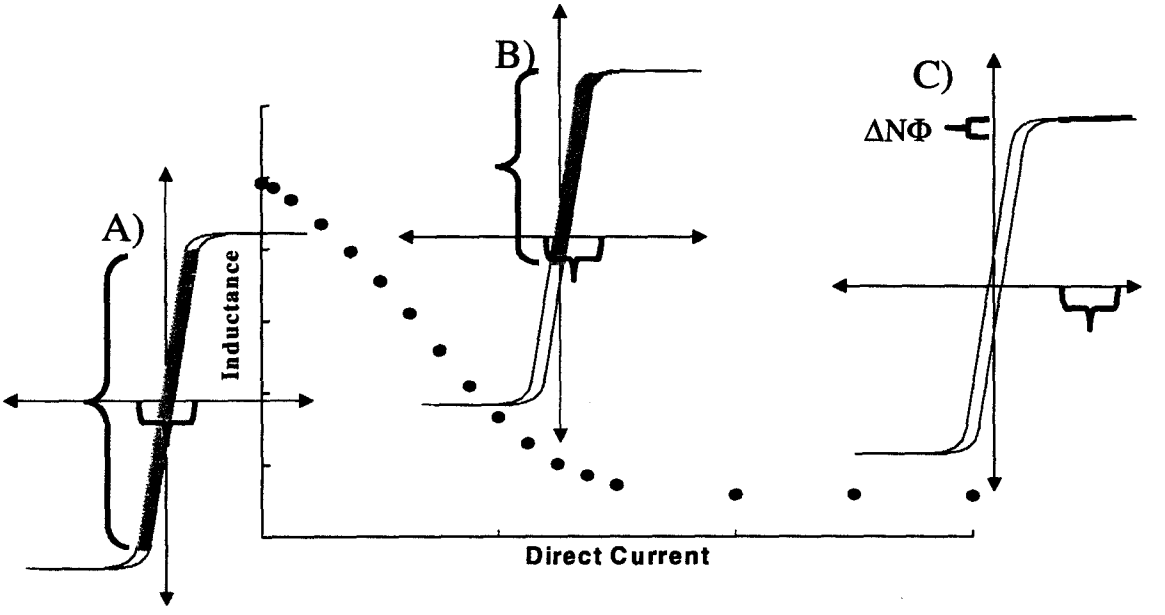

Figure 4 Inductance as a function of direct current for a typical magnetic core inductor. A) No dc bias, no saturation. B) partial saturation. C) complete saturation by the DC current.

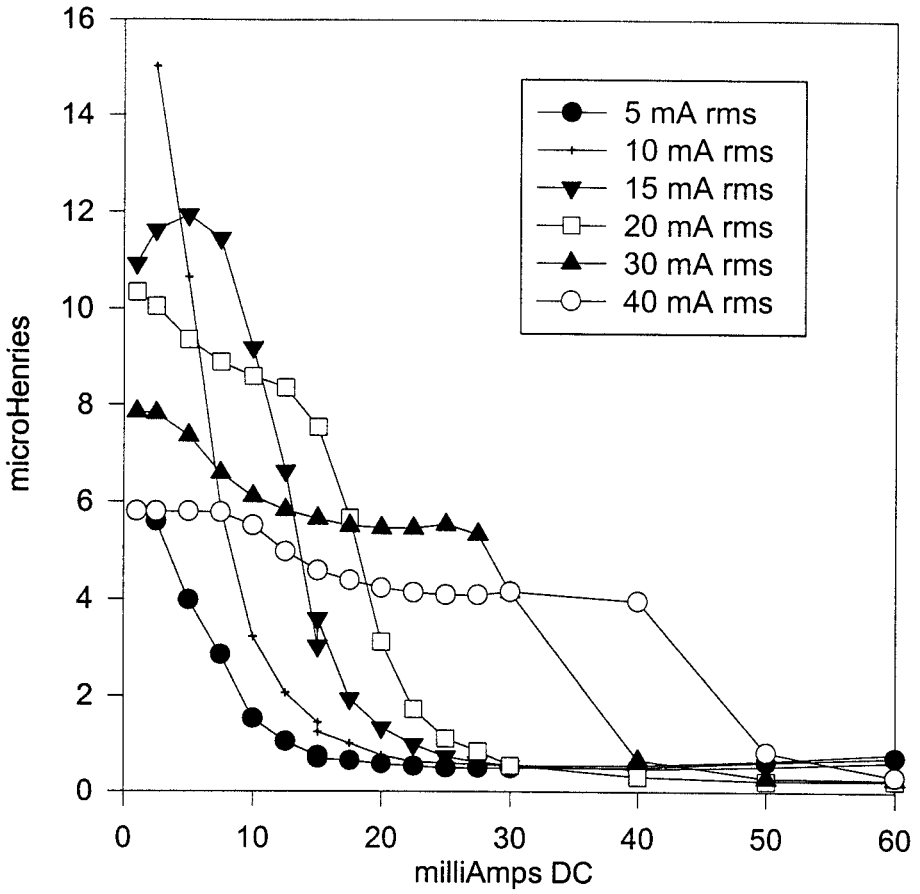

Figure 5 Inductance as a function of AC and DC current for an inductor. These particular data were measured on a gapped toroid microinductor at 1 kHz.

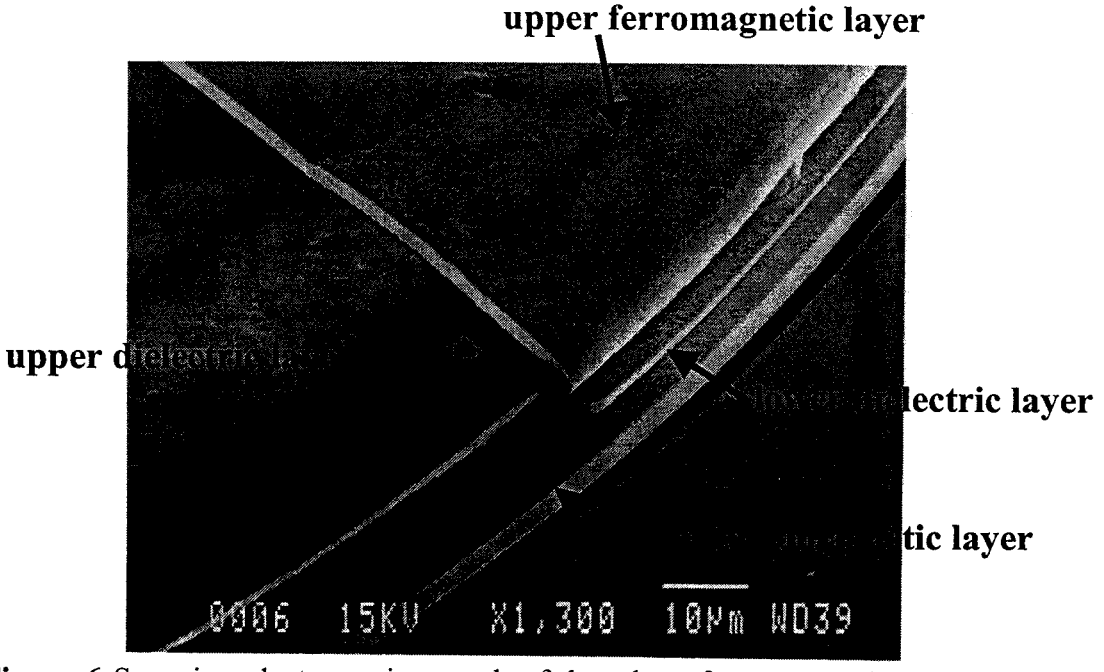

Figure 6 Scanning electron micrograph of the edge of an encapsulated spiral inductor. The lower dielectric layer creates a gap between the upper and lower ferromagnetic layers. The conductor is below the upper ferromagnetic layers, towards the upper left.

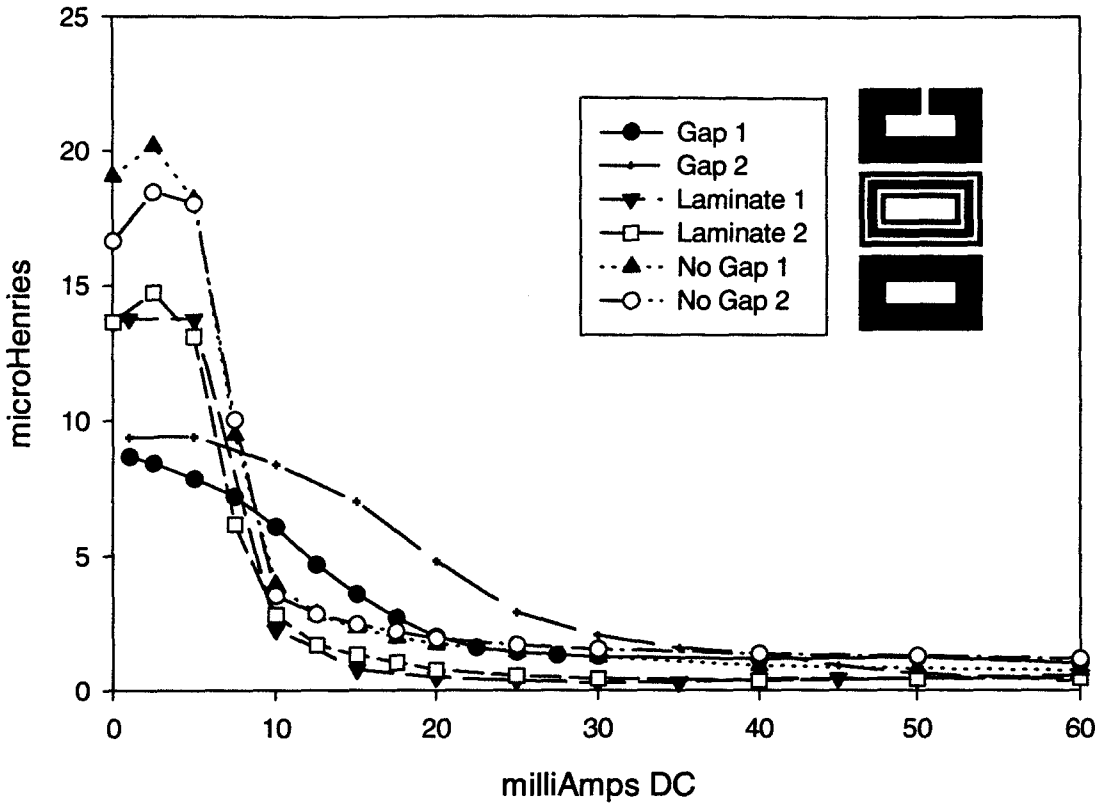

Figure 7 Inductance of several toroidal microinductors as a function of DC bias at 1 kHz, with 10 mA rms.

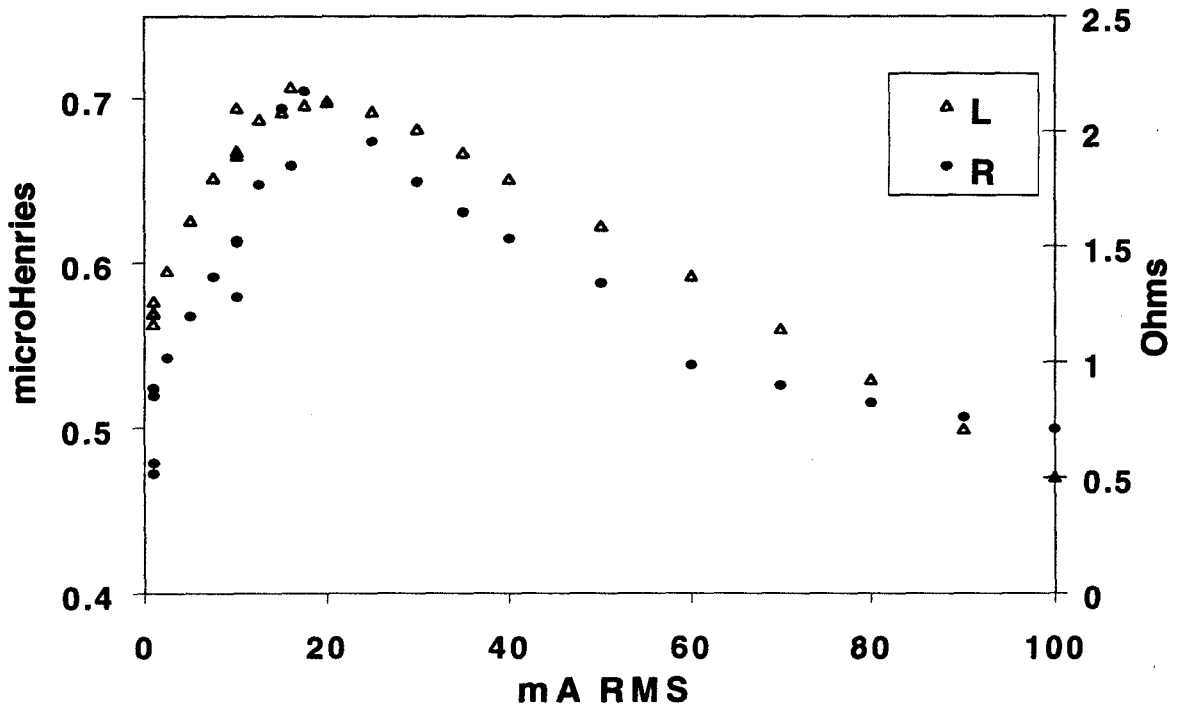

Figure 8 The inductance (open triangles) and the losses, "resistance", (solid circles) of one encapsulated spiral inductor with a ten-fold enhancement of its inductance over the value for its core alone. The frequency was 1 MHz.

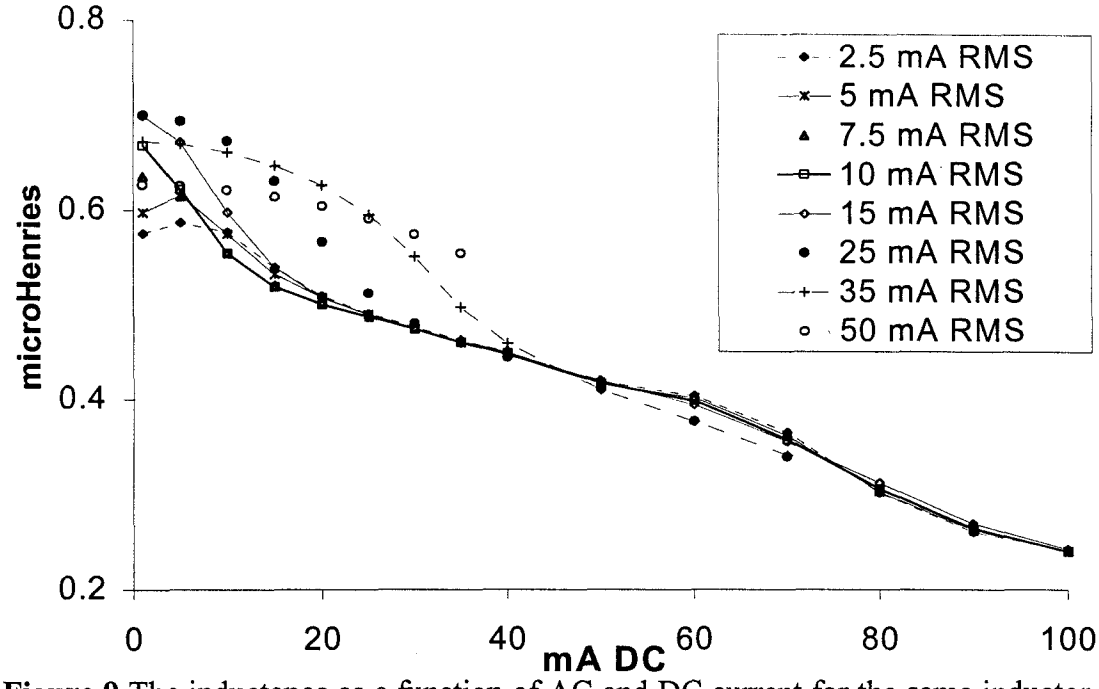

Figure 9 The inductance as a function of AC and DC current for the same inductor as in Figure 8 at 1 MHz.

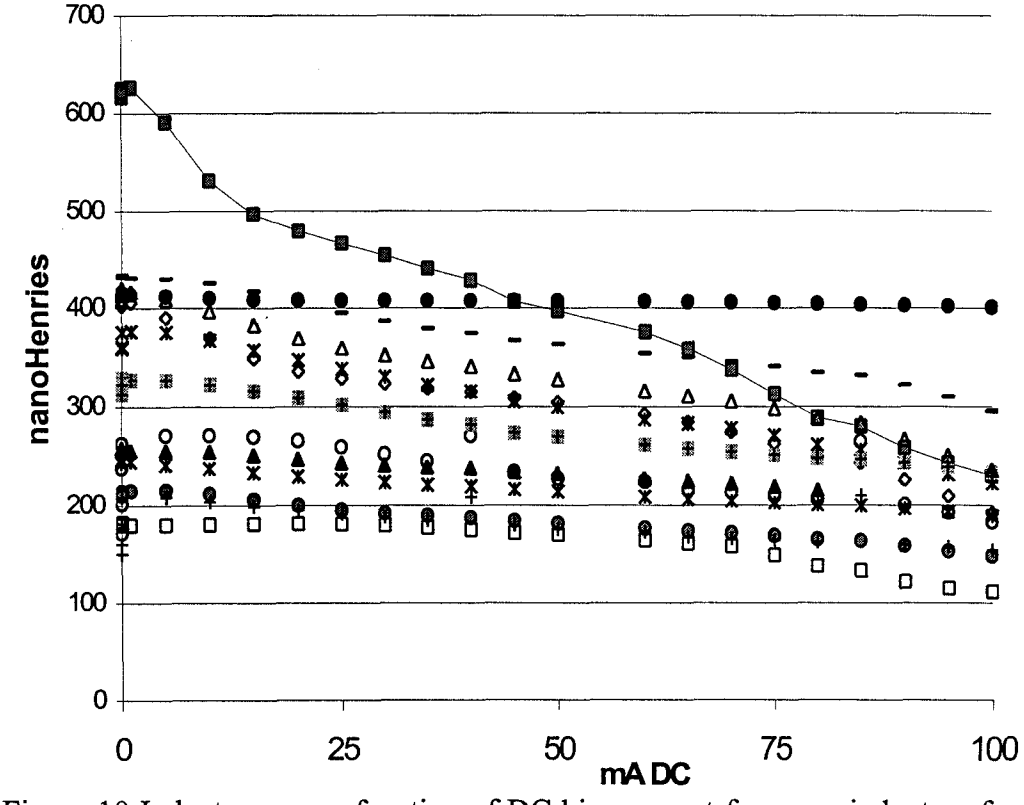

Figure 10 Inductance as a function of DC bias current for some inductors from one run. Measurements were made at 1 MHz with an alternating current of 10 mA rms. The solid circles (•) are data from an inductor with a 2 mm by 3 mm coil. All the rest have 0.6 mm^2 coils. The line highlights the data from the inductor featured in the previous plots.